INTERNATIONAL JOURNAL
ON INFORMATICS VISUALIZATION

journal homepage : www.joiv.org/index.php/joiv

Mixed Pixel Classification on Hyperspectral Image Using Imbalanced Learning and Hyperparameter Tuning Methods

Purwadi [a,b,*], Nor Azman Abu [b], Othman Bin Mohd [b], Bagus Adhi Kusuma [a]

[a] *Department of Informatics Engineering, Universitas AMIKOM Purwokerto, Purwokerto, Indonesia*
[b] *Pusat Teknologi Pengkomputeran Termaju, Fakulti Teknologi Maklumat dan Komunikasi, Universiti Teknikal Malaysia Melaka, Malaysia*
Corresponding author: [*]purwadi@amikompurwokerto.ac.id

Abstract—**Hyperspectral image technology in land classification is a distinct advantage compared to ordinary RGB and multispectral images. This technology has a wide spectrum of electromagnetic waves, which can be more detailed than other types of imagery. Therefore, with its hyperspectral advantages, the characteristics of an object should have a high probability of being recognized and distinguished. However, because of the large data, it becomes a challenge to lighten the computational burden. Hyperspectral has a huge phenomenon that makes computations heavy compared to other types of images because this image is 3D. The problem faced in hyperspectral image classification is the high computational load, especially if the spatial resolution of the image also has mixed pixel problems. This research uses EO-1 satellite imagery with a spatial resolution of 30 meters and a mixed pixel problem. This study uses a classification method to lighten the computational burden and simultaneously increase the value of classification accuracy. The method used is satellite image pre-processing, including geometric correction and image enhancement using FLAASH while the corrections are geometric correction and atmospheric correction. Then to lighten the computational burden, the steps carried out are using the Slab and PCA method. After obtaining the characteristics, they are entered into a guided learning model using a support vector machine (SVM) for the five-class or multiclass classification. Moreover, the imbalance learning method is proven to produce increased accuracy. The best results were achieved by the ADASYN method with an accuracy of 96.58%, while the computational time became faster with the feature extraction method.**

Keywords— **Mixed pixel; imbalanced learning; hyperparameter tuning, machine learning; hyperspectral classification.**

Manuscript received 19 Apr. 2023; revised 26 Jun. 2023; accepted 8 Jul. 2023. Date of publication 10 Sep. 2023.

I. INTRODUCTION

The capability of hyperspectral imaging technology to differentiate between hundreds of thousands of distinct colors makes this a reality. Due to the one-of-a-kind qualities of HSI data, the already challenging task of classifying hyperspectral images (HSI), which is the most difficult task in hyperspectral remote sensing, becomes even more complicated. It comprises a very large number of bands, all of which have significant correlations in the spectral domain and the spatial domain as a whole. In addition to this, there is a restricted amount of training available, which makes it even more challenging [1]

Hyperspectral has many more bands than multispectral does. In multispectral images, the number of spectra produced can range from 4 to 11, whereas in hyperspectral images, the number of spectra can range anywhere from tens to hundreds [2]. On the other hand, multispectral imagery has a drawback [3], which is that we cannot sequence images in real time concerning the amount of time the satellite is in orbit. Some situations need to be handled immediately, such as in a natural disaster; analysis that needs to be completed quickly can be accomplished with the help of hyperspectral images [4].

The hyperspectral image is first segmented into several homogeneous regions to obtain the class characteristics required to decompose mixed pixels. This enables the spectral and spatial features associated with each homogeneous region to be extracted. A single pixel in the remote-sensing image may represent multiple objects in the field. In addition, there are difficulties in recognizing and categorizing geographical features due to the overlap of two or more spectral properties connected to one another. Uncertainties, which point to a lack of classification accuracy, may be present in mixture cases [5].

Pixels, a mixture of several different types, are always the primary factor contributing to inaccurate classification results. Many different things can cause this. One of the primary factors that affect the improvement of classification

precision in images is the problem of mixed pixels. This is because each pixel contains two or more distinct ground information or intensity values. Using remote sensing images with a mixed pixel resolution is one of the valid assistance means that can be used to improve the quality of feature extraction from images. This can be done by using mixed-resolution remote sensing images. One of how image quality can be improved is through the use of this technique [6].

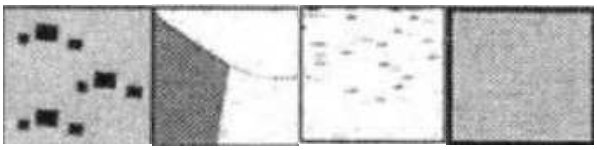

Fig. 1 Mixed Pixel Models

Images of this kind frequently have mixed pixels, which occurs when a single pixel covers several distinct ground surface types simultaneously [7]. As a direct consequence of this, the accuracy of the mapping will be impacted. Mapping at an extremely fine-grained resolution is another possibility that should be considered. Utilizing a technique known as super-resolution mapping is one approach that can remedy the issue of pixels containing a combination of distinct subtypes. This technique is also referred to as sub-pixel mapping in some circles. Following the percentage of the total area comprised of the land cover type in mixed pixels, a land cover type has been designated for each sub-pixel [8], [9].

Mixed pixels are always present, which is one of the primary challenges that must be overcome to achieve higher accuracy in land cover recognition and classification. Mixed pixels are always present in imagery acquired through remote sensing. In recent years, the technology known as spectral unmixing has been used to solve the problem of mixed pixels, improve the precision of tasks involving remote sensing classification, and more accurately identify the various types of land cover [10]

Mixed pixels are the name given to the pixels in the remote sensing image that contain information on various distinct objects with different resolutions. The primary factors that contribute to the formation of mixed pixels are as follows: the presence of small sub-pixel targets; mixing as a result of the pixel straddling the boundary of discrete thematic classes; gradual transition observation between continuous thematic classes; and mixing problem due to the contribution of a target. Besides, gradual transition observation between continuous and discrete thematic classes, gradual transition between continuous and discrete thematic classes, and mixing problems resulting from a target's contribution, can all play a role in forming mixed pixels [6].

One of the most difficult challenges faced in remote sensing is the classification of mixed pixel problems in satellite data. This is one of the most complex problems. When trying to identify mixed pixels, the blurriness of the image resolution is almost always a significant obstacle to overcome [11]. However, increasing the resolution of remote sensing images is one of the most important factors that can improve the image's quality when it comes to the extraction of features [6]. The impact of the low resolution of remote sensing data will restrict its application [12]. Some methods are done to increase the resolution, such as direct image synthesis, weighted average method, HIS transformation, principal component analysis, arithmetic combination based on Brovey transform, Gram-Schmidt transformation, and wavelet transform. The best improvement result was shown using Brovey transform for the segmentation remote sensing image [13].

The slab method is one way to divide a spectral into many segments that are all the same size. A slab is performed to search for local features if the area in question is homogenous. In earlier research, the spectra were extracted using the slab method, and the features used were the Modified Gaussian Model (MGM), represented in equation (1). This function computes three parameters: the center, the width, and the strength of the connection. It has been discovered that using this approach can result in an accuracy value of up to 70%. The hyperspectral image that was taken by the EO-1 satellite was the one that was used. It is possible to extract local area characteristics using statistical methods, such as the mean, median, minimum, maximum, skewness, and kurtosis[14].

Imbalance in a dataset is very common in the case of text classification. Dataset imbalance occurs when data in the minority class is dominated by the majority class, which causes the algorithm to not work properly to separate classes. To improve accuracy and performance results, datasets need to be balanced [15], [16], [17], [18]. The balancing methods that will be used in this study are Nearmiss, ADASYN (Adaptive Synthetic Sampling Approach), and SMOTE (Synthetic Minority Over-sampling Technique) [19] [20]. The Support Vector Machine (SVM) algorithm is used to create a model and see the performance of the balancing method used. Based on the literature obtained, this algorithm works quite well with imbalanced data conditions [19], [21].

ADASYN also helps reduce learning bias caused by uneven data distribution in the original dataset. The disadvantage of ADASYN compared to SMOTE is that the procedure is more complex and time-consuming due to its adaptive nature. The classifier combined with oversampling algorithms such as SMOTE and ADASYN can produce excellent classification results for balanced hyperspectral datasets. Also, the maximum total time consumed by ADASYN for all the classifiers [22].

One of the reasons why spectral mixing is one of the most serious issues is that Hyperion has a spatial resolution of thirty meters per pixel. This is one of the reasons why Hyperion has this resolution. The solution to this problem is to use only a subset of the bands that can be effectively utilized for spectral and subpixel mixture analysis. This will allow the problem to be circumvented. Because of this, it will be possible to simplify the challenge significantly. Because of the greater spectral separability of the various surface coverings, additional classification accuracy tends to be higher[23]. Homogeneity can be caused by 30 m/pixel, where each other has a similar spectral. So, it is difficult to differentiate the end member of spectral and find unique features for the classification of the pixel.

A hyperspectral image is made up of many different spectral bands that are adjacent to one another. Every pixel incorporates a continuous spectrum, which facilitates accurately recognizing various objects. Regarding image classification, the classifier's results are extremely dependent on the bands used. This is the case in almost every aspect of image classification. This is the case with binary as well as

pixel-based techniques for the classification of images. As a result of the fact that some of the bands are not informative and have a high degree of correlation, the percentage of pixels that are correctly classified is significantly reduced; because of this, a feature selection strategy that is flawless is required. The process of selecting features has as its primary goal the identification of an optimal subset of bands that will improve the classification accuracy [24].

Reducing high data dimensions to lower ones is a 'curse of dimension' problem. The dimensions of these changes tend to grow exponentially due to these events. High-dimensional data will result in a long processing time when processed directly and will typically require expensive costs. This is because of the high number of dimensions involved. Analysis techniques such as principal component analysis (PCA), linear discriminant analysis (LDA), and independent component analysis are just three examples of the methods that researchers used to reduce the number of dimensions in their data sets (ICA). Even without using principal component analysis (PCA), it is possible to create a useful classification for data that does not have an unusually large number of dimensions. This can be done when the number of dimensions is low. No guarantee that increasing the number of HSI pixel spectral features will result in a higher level of accurate pixel classification. For instance, in a technique for supervised classification, there comes a point where increasing the size of the input feature vector can further reduce the classification accuracy [25].

HSI classification has traditionally been regarded as a very difficult problem to solve due to the complex nature of the image scene (i.e., a large amount of data, mixed pixels, and a limited number of training samples). This is because there is a limited number of training samples available. Consequently, much work has been done in the past few decades to find an answer to this problem. Spectral-domain classifiers such as Supporting Vector Machines (SVM) have significantly improved the comprehension of image scenes during the early stages of HSI classification [26].

From the explanation above, it can be concluded that the problem that is the main focus of the research trend of hyperspectral image classification lies in the mixed pixel problem, directly proportional to the decrease in spatial resolution; it is more difficult to classify. As a result, developing a method for Mixed Pixel Classification on Hyperspectral Images is the primary focus of this research. In this research, the hyperspectral data collected by the Hyperion EO-1 was utilized. The techniques consisted of four steps; a.) data pre-processing satellite image; b.) imbalanced learning and Feature Extraction; c.) classification techniques and hyperparameter tuning; d.) performance evaluation methods.

II. Materials and Method

This chapter will elaborate on the method for classifying a hyperspectral resolution remote sensing image of Banyumas Regency, Indonesia. This study captures a hyperspectral scene image of the Latitude -7.4832 South and Longitude 109.1404 East with 14x41 pixels by Hyperion EO-1 Satellite using ENVI version 5.2 software. The subsequent procedures will be conducted radiometrically and geometrically. The purpose of radiometrically and geometrically correcting Hyperion EO-1 acquisition process errors. Hyperion EO-1 Hyperspectral Image will be classified using homogeneous region image classification to overcome the issues of mixed pixel-related land cover and identification. This proposed method will improve the accuracy of homogenous area imagery.

A. Unmixing Techniques

In Homogeneous Region techniques, the identity of known pixels will be grouped based on their specific Homogeneous Region values. While the mixed pixels or those of unknown identity are the remainders and classified as the overlapping pixel. The mixed pixel would create misclassification results in this research and need further analysis. Therefore, further analysis will resolve this issue using the proper Windows size, and the Homogeneous Region will be applied to obtain the final land use value. Therefore, this issue will be resolved by further analysis using the proper Windows size, and the Homogeneous Region will be applied to support the next process, the classification process. The process of land covers the classification process, as illustrated in Fig. 2.

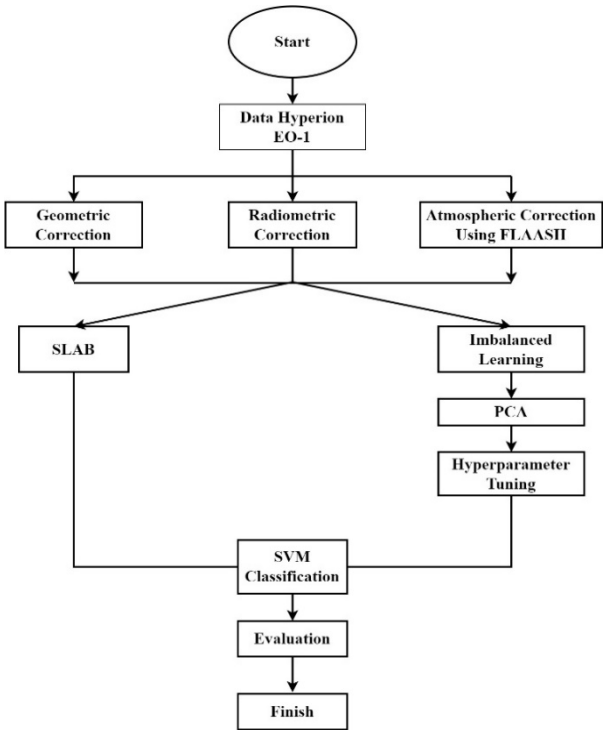

Fig. 2 Research methodology

B. Slab Techniques

In hyperspectral research, slabs are used to simplify computations and improve classification results, particularly on homogeneous images or images whose characteristics are relatively similar to each other and to those of other images. This is especially true for images with a high degree of similarity between themselves. In the current investigation, the picture is divided into several slab configurations, which will be examined using two to fifteen slabs. According to Patteti et al. [14], each Slab is an attribute for machine learning training.

The hyperspectral image, which is separated by using Slab, will be performed feature extraction. The feature extraction greatly determines the classification results, while the features used include mean, median, min, max, skewness, kurtosis,

amplitude, and standard deviation, where these features already represent some of the features found in the MGM method. The Slab divides the spectral area equally and extracts local features in the spectral [14], as shown in Fig. 3.

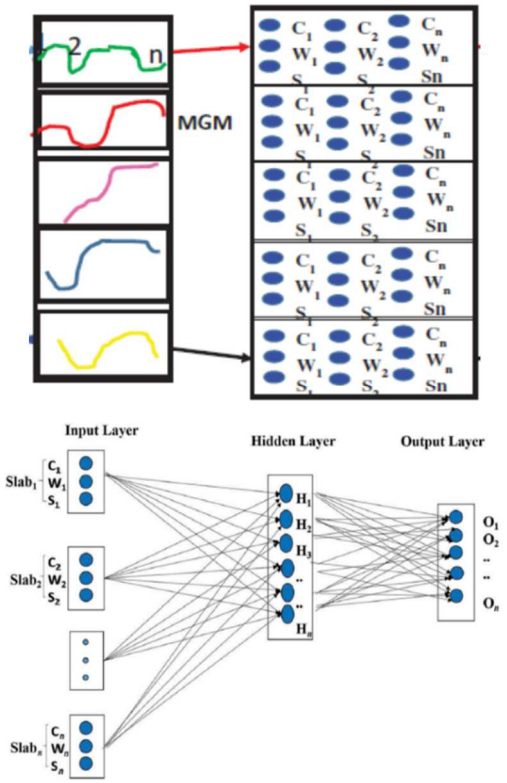

Fig. 3 Slab method

As shown in Fig. 4, each object has a different characteristic reflectance spectrum. The sensitivity of the reflection affects the spectral shape of the hyperspectral image. Of the 242 bands captured by the EO-1 hyperspectral image, sometimes parts of the band have significant characteristics that reflect a particular object. Therefore, by looking at each spectral' s local features, each object can have a good chance of being detected. Spectral EO-1 has the advantage of many bands compared to other satellite images. Therefore, every object should be detected properly using this image.

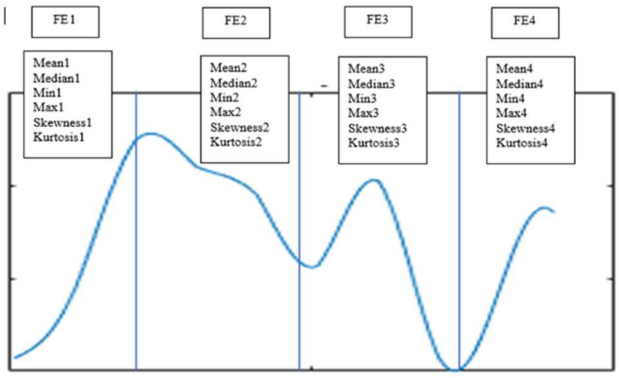

Fig. 4 Slab framework

SLAB, in this study, divides the spectral into several parts. Starting from two parts to 15 parts, each part is applied by feature extraction. Using the SLAB method, the features in each part of the spectrum will look more differentiated. Each SLAB will be concatenated and become a single matrix. The result of combining the features of each SLAB will be classified using SVM. The SLAB combination formula is shown in Eq. 1. Where FE_{tot} is the total feature extraction obtained from the concrete operation of each feature in each SLAB.

$$FEtot = [FE1 + FE2 + \ldots + FEn] \quad (1)$$

C. Feature Extraction on Hyperspectral Image

Often PCA is used as feature extraction for an unsupervised linear function. Extraction methods in reducing the dimensions of HSI and other remote sensing data. PCA-based methods can gather the most useful and best information for classification. In hyperspectral remote sensing images, PCA decides the correlation between bands to extract key HSI features. To deal with this, a PCA-based maximum noise fraction (MNF) transformation is introduced, in which the transformed features or principal components are classified based on maximization. Thus, the signal-to-noise ratio (SNR) does not differ as in the case of PCA and is optimal for use in HIS [27].

Remote sensing hyperspectral imaging (HSI) typically includes important land cover information obtained using A collection of hundreds of narrow, contiguous wavelengths [28]. Appropriate rating indicators can only provide the knowledge required for these massive HSI bands since the ranking result is incredible using all original features (ranges) from HSI. Although the essence is not easy to calculate features from ranges, range reduction (dimension) techniques through feature extraction and feature selection are commonly applied to increase the classification result and remove the curse of the dimensionality problem. Although Principal Component Analysis (PCA) is commonly used to reduce HSI features, it often does not extract useful HSI-local features for efficient classification where global HSI statistics are considered [29].

D. Classification of imbalanced Hyperspectral Image

An imbalanced learning method plays an important role in increasing accuracy. It is proven that by balancing, the accuracy results are better than before. The methods used are SMOTE, ADASYN, and Nearmiss. The SMOTE and ADASYN methods are types of balancing oversampling, while Nearmiss is a type of under sampling. Hyperparameter setting is very influential on the results of the classification. Therefore, several parameters will be set in this study, namely C, gamma, and epsilon. In addition, several kernels will be tested such as Gaussian and radial basis as well as standard kernels. If unsatisfactory, hyperparameter optimization can be tested with Grid Search method. The solution that is presented because of this research is to create a slab combination method, feature extraction, which makes the computation simpler. In addition to this, it modifies the parameters that are contained within the Support Vector Machine (SVM) algorithm, which can assist in enhancing the performance of classification.

III. Results and Discussion

The thresholding methods of mixed pixel problem classification obtained from high-resolution remote sensing images are discussed. Additionally, a comparison of the findings obtained from SLAB, Imbalanced Learning, Feature Extraction, and Hyperparameter Tunning based on the Support Vector Machine technique is included in this step. The next step in this research project is validating the accuracy of land identification through cross-validation and confusion matrix. The result that is considered acceptable will serve as the final threshold value for the mixed pixel categorization.

A. Data Pre-processing

The Banyumas district of Central Java, Indonesia, covers about 133,500 hectares. In this study, an area of 14 x 41 pixels in Banyumas District has been taken from the hyperspectral image of Hyperion EO-1 Satellite Data 2014 as training data. This process has been undertaken to avoid possible confusion in terms of spectral reflections between agricultural and non-agricultural crops, such as soil types, shadows, water, open land, and grasses in the study area. The extraction of 14 x 41 pixels satellite images is shown in Fig. 5.

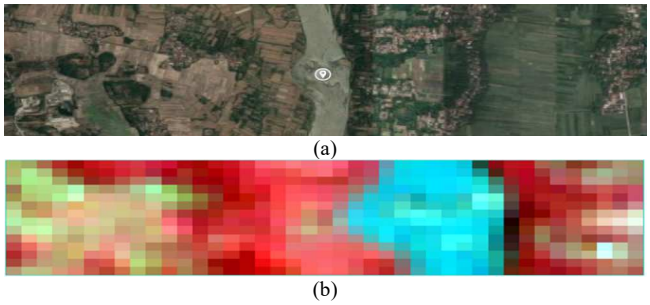

(a)

(b)

Fig. 5 (a) True Color Image, (b) The 14 x 41 pixels of satellite image

B. Training Data Scenario

Training data plays an important role in the classification results. Some of the classification problems start with training data. For example, imbalance data occurs when there is an imbalance in training data in one class only in multiclass classification. The training data tested in this study used the cross-validation method with varying K values. The cross-validation method makes the training data array automatically balanced. Using k-fold, the accuracy values will be averaged in each data-splitting scenario.

The data is separated between the training and validation sets according to the specified K value. If the value of K is equal to 2, then the amount of training data compared to validation data is 50:50. The equations to determine the amount of training data and validation data are as shown in equations 2 and 3. Data other than the validation set are not reused for the training set in each iteration. However, in subsequent iterations, the data that was once the validation set will be used as training data. Classification in each fold will get an accuracy value; later, each accuracy value in each iteration will be averaged.

$$val.set = \frac{AllData}{k} \quad (2)$$

$$Train.set = exp\ (val.set) \quad (3)$$

In addition, the preparation for the training sample includes a few different practices that can be utilized in order to achieve better results. Many data sets have significant class imbalances, meaning that one or a few classes dominate the labels. One easy option would be to weigh them according to the loss function to penalize the classes that appear less frequently with a greater degree of severity. For this purpose, the inverse-median frequency class weighting method is frequently applied as an example in semantic segmentation. This is the same as providing the model with additional examples from the less common classes [30].

C. Slab Results and Analysis

Classification of hyperspectral images has challenges, especially the characteristics of images with spectral similarities make the classification model difficult to detect. The smaller the spatial resolution, the more mixed pixels that occur there, so special techniques are needed to overcome this, plus areas with similarities, such as rice fields with forests, few residential areas, or roads that mix with vegetation, create complex problems in classification. This study classified it into five classes: house, road, trees, river, and paddy field.

TABLE I
SLAB and K-FOLD Test Results

No.	SLAB	KFOLD				Average	Std Dev	Gap value
		2	4	5	10			
1	2	50.52	50.7	48.95	50.17	50.09	0.79	1,75
2	3	50.35	50	50.17	50	50.13	0.17	0,35
3	4	48.61	49.83	49.83	50.35	49.66	0.74	1,74
4	5	49.13	49.65	48.95	49.65	49.35	0.36	0,70
5	6	47.04	48.08	49.13	47.04	47.82	1.00	2,09
6	7	47.04	48.26	49.13	50.35	48.70	1.40	3,31
7	8	46.34	48.43	48.08	48.61	47.87	1.04	2,27
8	9	49.48	47.91	48.08	49.13	48.65	0.77	1,57
9	10	47.21	47.73	47.39	47.73	47.52	0.26	0,52
10	11	45.82	47.39	47.91	48.43	47.39	1.13	2,61
11	12	46.17	47.04	47.73	47.39	47.08	0.67	1,56
12	13	44.42	45.64	46.52	45.64	45.56	0.86	2,10
13	14	45.82	47.56	45.99	48.78	47.04	1.40	2,96
14	15	46.86	46.86	46.86	46.86	46.86	0.00	0,00
Average		47,49	48.22	48.19	48.58	48.12	0.76	1.68
Std. Dev		1,84	1.40	1.24	1.48	1.35	0.43	0.99

Some parameter settings are done by setting the order polynomial value, kernel function, and kernel scale. From the test results, the test table is obtained as follows. The slab process is also carried out at each stage of the training data and adjusts to the k-fold configuration used. The results of testing variations in parameter settings, Slab, and k-fold can be seen in the following Table I. The highest accuracy value in SLAB 2 KFOLD 4 is 50.7, while for the smallest SLAB 13 KFOLD 2 is 44.42. The highest average accuracy value in SLAB 3 is 50.13, while the smallest SLAB 13 is 45.56.

The k-fold test showed that the more the value of k, the lower the accuracy trend. Likewise, with the addition of slabs, the more slabs there are the lower the accuracy. The optimal average slab value equals 3, while the optimal average k-fold value is k=4. The standard deviation value of the smallest slab variation is 0.00 using slab 15, while the largest is slab 7 and slab 14. From the results, it can be seen that the recommended slab use is slab 2 and with a value of k=4. The average value of the standard deviation is 0.76, which can still be considered, but it is necessary to improve the accuracy of the

results. While for the smallest gap value is by using slab 15 of ±0.00 and the largest gap value is by slab 7 with a value of ±3.31. This shows that the best result is to use slab 2. In testing using SLAB 2 Kfold 4 using Linear Kernel, Gaussian, RBF, Polynomial combined with Polynomial Orders 2 to 10, the highest and lowest values obtained from each Kernel are as follows in Table II.

TABLE II
KERNEL AND POLYNOMIAL ORDER

Kernel	Polynomial Order									Std. Dev.	Avg.
	2	3	4	5	6	7	8	9	10		
Linear	50	48.43	49.83	50.35	50.17	50.35	51.39	50.70	50.17	0.79	50.15
Gaussian	49.48	50.70	50	49.30	50.35	50.17	51.39	50	50.70	0.65	50.23
RBF	49.83	50.87	50.17	48.78	50.35	49.48	50.87	49.48	49.65	0.69	49.94
Polynomial	50.52	50.52	50.17	49.13	50	50.35	50.52	49.30	50.35	0.53	50.10

Based on the standard deviation measurement of the tested Kernel, the best value obtained is using the Polynomial kernel, where the Polynomial kernel is the most stable compared to other kernels but has an accuracy that is still below other kernels. The use of a polynomial kernel because the polynomial model has good curve fitting flexibility when compared to the others, which is 50.23%, but the highest result is still achieved by using a linear kernel using order 8 with an accuracy of 51.39% even though the standard deviation is 0.65. Testing using the Gaussian Kernel also has the same accuracy as the linear Kernel of order 8 polynomial, which is 51.39%. However, the use of kernels that can be recommended in this study is to use linear and Gaussian kernels, even though they have an average value below the polynomial Kernel, but it is not so significant because it is only 0.8% adrift. In SLAB 2 and K-fold 4, which are the highest classification results, 50.7, the CM evaluation results are seen in Table III and Fig. 6.

TABLE III
RESULTS OF CM SLAB 2 K-FOLD 4

Class	Label Description	True	False
1	Houses	0	33
2	Road	0	6
3	Tree	261	29
4	River	0	119
5	Paddy	22	104

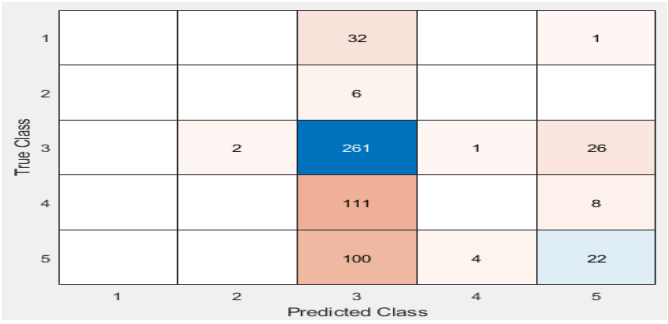

Fig. 6 Results of CM SLAB 2 K-fold 4

At SLAB 13 and K-fold 2, which are the lowest classification results 44.42, the results of the CM evaluation are as follows in Table IV and Fig. 7.

TABLE IV
RESULTS OF CM SLAB 13 K-FOLD 2

Class	Label Description	True	False
1	Houses	1	32
2	Road	0	6
3	Tree	223	67
4	River	11	108
5	Paddy	20	106

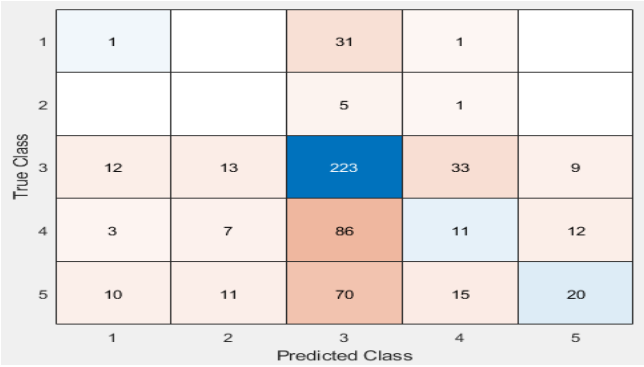

Fig. 7 Results of CM SLAB 13 K-fold 2

When setting the optimization hyperparameters, exercising extreme caution is the most important. The findings of the test will be overly positive. If this cannot be accomplished, cross-validation that includes multiple trains and test splits is an effective method for determining the degree to which the hyperparameters resist overfitting. In conclusion, while conducting inference, it is preferable to use the network that achieved the best validation score rather than the weights from the most recent epoch because those weights may not always be accurate. This indicates that checkpoints should be saved at regular intervals throughout the training. We did our best in our toolbox to adopt these best practices while allowing sophisticated users to use their own settings whenever necessary[30].

D. Spectral Analysis

The hyperspectral image at a spatial resolution of 30m has many constraints, where the image with that specification contains several objects in one pixel, also called mixed pixel. A spatial resolution of 30m means that in one pixel measuring 30x30 meters there are many objects, because with that size, it could consist of many objects. For example, the river class will merge with the rice field class, or the rice field class can merge or mix with the tree class. As a result of the phenomenon, spectra that have mixed pixels can have the same chance.

An image with many objects in one pixel has a different shape than a pure class pixel or a spectral endmember. The mold used to determine the spectral class is from the shape of the endmember, where the spectral to be recognized will be checked for similarity with the spectral endmember, which is pure in nature. This end member is taken from an algorithmic determination using the PPI (Pure Purity Index) method. Suppose it is observed that there is a difference in the curve of each class, which class can be searched for the latest data

based on the end member reference. Ambiguous data is mixed pixel data shown in the following Fig. 8.

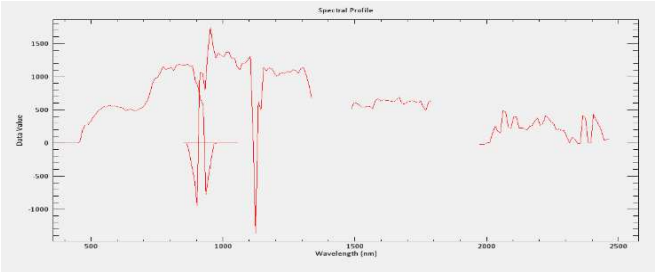

Fig. 8 Example Mixed pixel river with trees

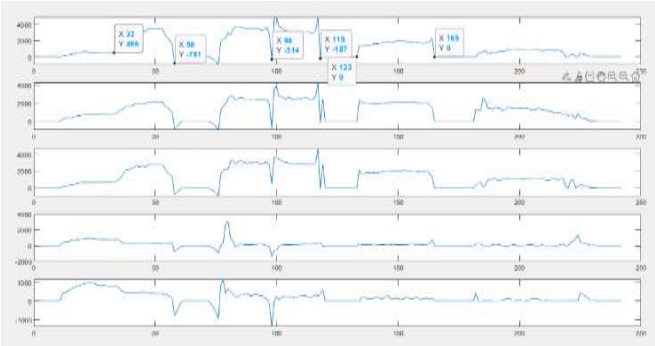

Fig. 9 The difference in the characteristics of each class

The results of the comparison plotting are displayed in Fig. 9, and it can be seen that classes 1, 2, 3, 4, and 5 all have similar curve shapes; the only difference is in the amplitude. When applied to the data, this curve allows the class to be segmented into two groups—namely, land and water. Bands 33–58, 98–108, and 133–165 are the ranges of bands that best represent the two distinct clusters, as revealed by the shape of the curve. This may also be deduced from bands 33–58, 98–108, and 133–165 form the bulk of the curve. Because of this, differentiating between the two clusters is made simpler, but separating each cluster requires additional procedures. It is possible to conclude that the procedure for classifying the five classes can be initiated by first classifying the two classes. The two-class clustering approach can be carried out solely by considering the degree to which the values of the curves in a band are comparable. This allows for the slab division to be conducted in a manner that is tailored to the bands described earlier.

The mean, the minimum, the maximum, and the standard deviation are the variables that can be employed. These values are then applied to each custom slab, and the result is that each Slab characterizes the class in question based on a statistically generated curve. Examining the global values from bands 1 to 242 results in the following table, which is an illustration of feature extraction. Introducing new classes or categorizing existing classes might use custom slabs as characteristics in the subsequent stage of the process. This categorization method can be utilized for mixed pixel pre-processing, as it consists of 10 combinations of five different classes that each correlate to a one-to-one connection. The separation of fellow clusters, where the training data has a significantly distinct curve shape, is one of the notes that need further research; this difficulty can be avoided using the moving average method. The noise that is present in each band is first removed, and then the curve is smoothed. The ground truth curves, and training data are incorporated into the smooth curves. As a result, the two curves are moved and averaged together before determining the degree of similarity.

E. Hyperspectral Classification by IL and PCA.

The result from RAW data has been tested, as shown in Table V, and the results are not satisfied yet. An imbalanced learning method plays an important role in increasing accuracy. It is proven that the accuracy results are better than before by balancing. The methods used are SMOTE, ADASYN and Nearmiss. The SMOTE and ADASYN methods are types of balancing oversampling, while Nearmiss is a type of under sampling. From the test results, it can be obtained that ADASYN achieves the best value, then SMOTE, and lastly, by using Nearmiss. The evaluation value produced by the Nearmiss method is very poor because the data generated from the balancing process is very small, while ADASYN, according to theory, is a complement to SMOTE as evidenced by achieving the highest score is 96.58%, as shown in the following table V – VIII.

TABLE V
ACCURACY RESULT FROM RAW DATA

SPLIT	RAW	RAW + Hyperparameter	RAW + PCA				Hyperparameter + PCA + RAW			
			20	15	10	5	20	15	10	5
70:30	0.7980	0.7849	0.8179	0.8179	0.8204	0.7980	0.7326	0.7616	0.7384	0.7558
80:20	0.8013	0.8348	0.8035	0.8035	0.7947	0.7904	0.7130	0.7478	0.6783	0.7391
90:10	0.7981	0.8448	0.8058	0.8058	0.8019	0.7883	0.7241	0.7586	0.7586	0.7241

TABLE VI
ACCURACY RESULT FROM SMOTE DATA

Accuracy	SMOTE	SMOTE + Hyperparameter	SMOTE + PCA				Hyperparameter + SMOTE + PCA			
			20	15	10	5	20	20	15	5
70:30	0.8463	**0.9586**	0.8877	0.9596	70:30	0.8463	**0.9586**	0.8877	0.9596	70:30
80:20	0.8473	0.9471	0.8788	0.8739	80:20	0.8473	0.9471	0.8788	0.8739	80:20
90:10	0.8433	0.9379	0.8768	0.8581	90:10	0.8433	0.9379	0.8768	0.8581	90:10

TABLE VII
ACCURACY RESULT FROM ADASYN DATA

Accuracy	ADASYN	ADASYN + Hyperparameter	ADASYN + PCA				Hyperparameter + ADASYN + PCA			
			20	15	10	5	20	15	10	5
70:30	0.8309	**0.9658**	0.8699	0.8553	0.8231	0.8035	0.9362	0.9362	0.9179	0.8907
80:20	0.8133	0.9453	0.8651	0.8524	0.8211	0.7996	0.9453	0.9430	0.9362	0.8769
90:10	0.8309	0.9635	0.8729	0.8631	0.8240	0.8084	0.9476	0.9294	0.9179	0.8679

TABLE VIII
ACCURACY RESULT FROM NEARMIS DATA

Accuracy	Near Miss	Near Miss + hyperparameter	Near Miss + PCA				Hyperparameter + Near Miss + PCA			
			20	15	10	5	20	15	10	5
70:30	0.6190	0.3333	0.8571	0.8571	0.8571	0.7619	0.2222	0.2222	0.333	0.444
80:20	0.6190	0.3333	0.8571	0.8571	0.8571	0.7619	0.2222	0.2222	0.444	0.333
90:10	0.6190	0.3333	0.8571	0.8571	0.8571	0.7619	0.2222	0.2222	0.444	0.333

F. Parameter Tuning of Hyperspectral Classification

In this research, we applied Grid Search for hyperparameter tuning in support vector machines. The results show that by adding hyperparameter tuning, the accuracy of classification was improved. Several parameters have been tuned: Regularization (C), kernels (rbf, polynomial, sigmoid, linear) with degrees 1 to 6. The highest accuracy score of 0.9658 was achieved by using ADASYN with 70:30 data splitting, as shown in Table VII. The best Kernel is linear, the degree value is 1, and regularization C = 1000

G. Training Time Consuming

We tested the training computation time on raw data and data that has been done by PCA, which is divided into four test scenarios, namely raw data, SMOTE data, ADASYN, and Nearmiss, as shown in table IX-XII. The results show that PCA will reduce time consumption (in seconds), showing significant differentiation. The order of training computation speeds starting from the slowest is ADASYN, SMOTE, Raw, and Nearmiss. However, ADASYN achieved the best accuracy with a training computation time of 53.2889 seconds.

TABLE IX
RAW TRAINING COMPUTATION TIME

SPLIT	RAW	RAW + Hyperparameter	RAWPCA				Hyperparameter + PCA			
			20	15	10	5	20	15	10	5
70:30	0.0155	10.8465	0.0099	0.0076	0.0069	0.0077	7.1596	0.7616	5.4574	7.8451
80:20	0.0151	12.0788	0.0094	0.0092	0.0099	0.0076	7.4964	7.5763	7.3613	10.0592
90:10	0.0468	15.3894	0.0391	0.0259	0.0099	0.0098	9.1987	8.0742	8.1898	13.0369

TABLE X
SMOTE TRAINING COMPUTATION TIME

SPLIT	SMOTE	SMOTE + Hyperparameter	SMOTE + PCA				Hyperparameter + PCA + SMOTE			
			20	15	10	5	20	15	10	5
70:30	0.0614	42.6989	0.0219	0.0320	0.0225	0.0222	338.8842	395.0979	950.4286	76.7342
80:20	0.0578	37.6438	0.0255	0.0222	0.0233	0.0201	411.5554	343.7659	831.8402	534.2155
90:10	0.0489	33.9573	0.0397	0.0262	0.0236	0.0192	467.4475	413.6568	553.7054	587.2017

TABLE XI
ADASYN TRAINING COMPUTATION TIME

SPLIT	ADASYN	ADASYN + Hyperparameter	ADASYN + PCA				Hyperparameter + PCA + ADASYN			
			20	15	10	5	20	15	10	5
70:30	0.0895	**53.2889**	0.0376	0.8553	0.0296	0.0283	**0.9362**	0.9362	0.9179	0.8907
80:20	0.0886	57.4781	0.0361	0.0379	0.0267	0.0288	539.1479	840.4484	1170.3905	776.1726
90:10	0.0998	52.4546	0.0291	0.0281	0.0271	0.0249	599.1084	637.8602	894.9696	758.5352

TABLE XII
NEARMISS TRAINING COMPUTATION TIME

SPLIT	Near Miss	Near Miss + hyperparameter	Near Miss + PCA				Hyperparameter + PCA + Near Miss			
			20	15	10	5	20	15	10	5
70:30	0.0051	2.8687	0.0012	0.0019	0.0025	0.0012	1.0371	1.0289	1.0209	1.0468
80:20	0.0044	2.8698	0.0014	0.0018	0.0028	0.0019	1.1302	0.9884	1.0385	0.9948
90:10	0.0066	3.0068	0.0038	0.0025	0.0011	0.0018	1.0482	1.0445	1.0489	1.0749

H. Testing Time Consuming

In Table XIII - XVI are the results of time-consuming (in seconds) testing data, and the order of training computation speed starting from the slowest are ADASYN, SMOTE, Raw, and Nearmiss, with the best accuracy time, is 0.8223 seconds reached by ADASYN 70:30.

TABLE XIII
RAW TESTING COMPUTATION TIME

SPLIT	RAW	RAW + PCA			
		20	15	10	5
70:30	0.0082	0.0034	0.0021	0.0019	0.0017
80:20	0.0068	0.0025	0.0022	0.0036	0.0015
90:10	0.0065	0.0104	0.0052	0.0010	0.0010

TABLE XIV
SMOTE TESTING COMPUTATION TIME

SPLIT	SMOTE	SMOTE + PCA			
		20	15	10	20
70:30	0.0515	0.0139	0.0136	0.0137	0.0139
80:20	0.0356	0.0151	0.0139	0.0129	0.0122
90:10	0.0345	0.0184	0.0157	0.0117	0.0123

TABLE XV
ADASYN TESTING COMPUTATION TIME

SPLIT	ADASYN	ADASYN + PCA			
		20	15	10	20
70:30	0.0600	0.0184	0.0168	0.0196	0.0209
80:20	0.0585	0.0212	0.0189	0.0176	0.0150
90:10	0.0668	0.0178	0.0176	0.0147	0.0131

TABLE XVI
NEARMISS TESTING COMPUTATION TIME

SPLIT	ADASYN	ADASYN + PCA			
		20	15	10	20
70:30	0.0029	0.0002	0.0032	0.0005	0.0003
80:20	0.0032	0.0008	0.0003	0.0003	0.0002
90:10	0.0036	0.0006	0.0009	0.0003	0.0038

I. Mixed Pixel Data Distribution Analysis

Mixed pixels are a problem for hyperspectral data classification. The way to see if data contains overlapping classes is to measure it with the T-distributed Stochastic Neighbor Embedding (tSNE) [31], [32]. Figure 10 shows the tSNE values using different distance measurement methods: Mahalanobis, Cosine, Euclidian, and Chebyshev. The results show overlapping data, which also means a mixed pixel problem.

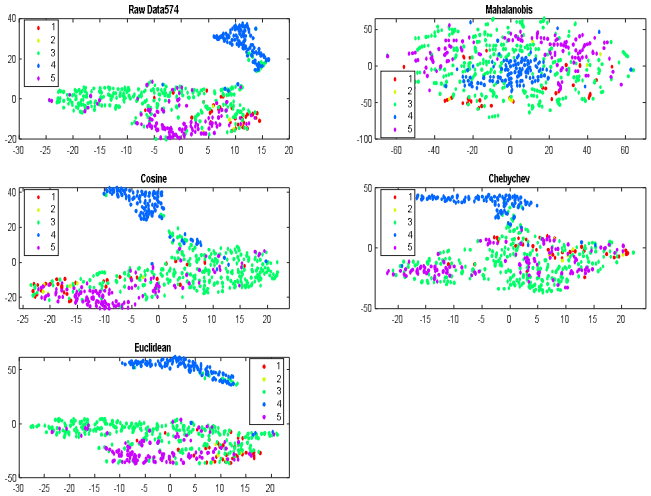

Fig. 10 tSNE from raw data hyperspectral

IV. CONCLUSION

The high operational costs of hyperspectral lead the spatial resolution to have problems with mixed pixel, which in turn causes the classification results to be worse than they otherwise would be. Based on these issues, improving the classification results requires multiple strategies, specifically picture pre-processing, pre-processing, and changing parameters on the classification model.

The usage of the slab method proves to be more effective in terms of speed as well as the strain placed on the computer resources. Slab directly decreases the image's dimensions, and while the image had 574 data before it was reduced, it now has dimensions that are 0.045% of the size of the original image after passing through the slab 2 procedure. As a result, it has been demonstrated that making use of slabs in this research can ease the strain of computing work in a significantly more effective manner.

Pre-processing, which includes geometric correction, FLAASH, and Slab, is used to improve the accuracy of the results. Pre-processing also improves the speed of calculation. The best classification results that could be obtained were 50.7% while utilizing Slab 2 configuration, polynomial order 2, linear SVM kernel, and using k-fold 4 as the fold factor. The slab 2 method produces results with an accuracy average of 50.09 percent. These findings have been deemed satisfactory for the hyperspectral data despite mixed-pixel problems.

The results of the classification test show that the imbalance learning method is proven to produce increased accuracy. The best results were achieved by the ADASYN method with an accuracy of 96.58% using hyperparameter data without PCA. While accuracy using PCA achieved decreased results, namely 93.62%. These results experienced a decrease in accuracy of 2.96%, but the computational training time was reduced from 53.2889 to 0.9362, indicating an increase in computational speed of 56.92 times faster. Whereas the previous testing data was 0.82 seconds, after PCA, it was 0.84 seconds, so the testing time was not so influential.

ACKNOWLEDGMENT

The authors thank the financial support from Universitas AMIKOM Purwokerto and Universiti Teknikal Malaysia Melaka for their assistance in this research.

REFERENCES

[1] S. Bera and V. K. Shrivastava, "Analysis of various optimizers on deep convolutional neural network model in the application of hyperspectral remote sensing image classification," *Int J Remote Sens*, vol. 41, no. 7, pp. 2664–2683, Apr. 2020, doi: 10.1080/01431161.2019.1694725.

[2] L. Su, Y. Sui, and Y. Yuan, "An Unmixing-Based Multi-Attention GAN for Unsupervised Hyperspectral and Multispectral Image Fusion," *Remote Sens (Basel)*, vol. 15, no. 4, Feb. 2023, doi: 10.3390/rs15040936.

[3] K. Zhang *et al.*, "Panchromatic and multispectral image fusion for remote sensing and earth observation: Concepts, taxonomy, literature review, evaluation methodologies and challenges ahead," *Information Fusion*, vol. 93. Elsevier B.V., pp. 227–242, May 01, 2023. doi: 10.1016/j.inffus.2022.12.026.

[4] Purwadi, N. Suryana, and N. A. Abu, "An understanding rice hyperspectral remote sensing imagery classification framework," *J Theor Appl Inf Technol*, vol. 97, no. 3, pp. 879–896, 2019.

[5] Purwadi, N. Suryana, N. A. Abu, and B. A. Kusuma, "A comprehensive review: Classification techniques on hyperspectral remote sensing," *International Journal of Advanced Trends in Computer Science and Engineering*, vol. 8, no. 1.5 Special Issue, pp. 156–164, 2019, doi: 10.30534/ijatcse/2019/3181.52019.

[6] N. Gupta and V. K. Panchal, "Artificial intelligence for mixed pixel resolution," *International Geoscience and Remote Sensing Symposium (IGARSS)*, pp. 2801–2804, 2011, doi: 10.1109/IGARSS.2011.6049796.

[7] B. Fang, Y. Bai, and Y. Li, "Combining spectral unmixing and 3D/2D dense networks with early-exiting strategy for hyperspectral image classification," *Remote Sens (Basel)*, vol. 12, no. 5, Mar. 2020, doi: 10.3390/rs12050779.

[8] L. Li, T. Xu, and Y. Chen, "Improved urban flooding mapping from remote sensing images using generalized regression neural network-based super-resolution algorithm," *Remote Sens (Basel)*, vol. 8, no. 8, 2016, doi: 10.3390/rs8080625.

[9] C. Zhang, Q. Wang, H. Xie, Y. Ge, and P. M. Atkinson, "Spatio-temporal subpixel mapping with cloudy images," *Science of Remote Sensing*, vol. 6, p. 100068, Dec. 2022, doi: 10.1016/j.srs.2022.100068.

[10] S. Wu *et al.*, "Influence of reconstruction scale, spatial resolution and pixel spatial relationships on the sub-pixel mapping accuracy of a double-calculated spatial attraction model," *Remote Sens Environ*, vol. 210, pp. 345–361, Jun. 2018, doi: 10.1016/j.rse.2018.03.015.

[11] K. Mahata, R. Das, S. Das, and A. Sarkar, "Automatic Mixed Pixel Detection using a new Hybrid Cellular Automata Approach on Satellite Image," in *2017 1st International Conference on Electronics, Materials Engineering and Nano-Technology (IEMENTech)*, 2017.

[12] X. Meng, H. Shen, H. Li, Q. Yuan, H. Zhang, and L. Zhang, "Improving The Spatial Resolution of Hyperspectral Image Using Panchromatic and Multispectral Images : An," in *Hyperspectral Image*

and Signal Processing: Evolution in Remote Sensing (WHISPERS), 2015 7th Workshop on, 2015, pp. 1–4.

[13] A. Hryvachevskyi, I. Prudyus, L. Lazko, and S. Fabirovskyy, "Improvement of segmentation quality of multispectral images by increasing resolution," *Proceedings of 2016 17th International Conference Computational Problems of Electrical Engineering, CPEE 2016*, pp. 2–5, 2016, doi: 10.1109/CPEE.2016.7738750.

[14] S. Patteti, B. Samanta, and D. Chakravarty, "Design of a feature-tuned ANN model based on bulk rock-derived mineral spectra for endmember classification of a hyperspectral image from an iron ore deposit," *Int J Remote Sens*, vol. 36, no. 8, pp. 2037–2062, Apr. 2015, doi: 10.1080/01431161.2015.1031920.

[15] W. Feng, W. Huang, H. Ye, and L. Zhao, "Synthetic Minority Over-Sampling Technique Based Rotation Forest For The Classification Of Unbalanced Hyperspectral Data," in *IGARSS 2018-2018 IEEE International Geoscience and Remote Sensing Symposium*, IEEE, 2018, pp. 2651–2654.

[16] D. Datta *et al.*, "A Hybrid Classification of Imbalanced Hyperspectral Images Using ADASYN and Enhanced Deep Subsampled Multi-Grained Cascaded Forest," *Remote Sens (Basel)*, vol. 14, no. 19, Oct. 2022, doi: 10.3390/rs14194853.

[17] W. Feng, W. Huang, and W. Bao, "Imbalanced Hyperspectral Image Classification with an Adaptive Ensemble Method Based on SMOTE and Rotation Forest with Differentiated Sampling Rates," *IEEE Geoscience and Remote Sensing Letters*, vol. 16, no. 12, pp. 1879–1883, Dec. 2019, doi: 10.1109/LGRS.2019.2913387.

[18] J. F. R. Rochac, N. Zhang, L. Thompson, and T. Oladunni, "A Data Augmentation-Assisted Deep Learning Model for High Dimensional and Highly Imbalanced Hyperspectral Imaging Data," in *9th International Conference on Information Science and Technology : ICIST2019 final program*, 2019, pp. 362–367.

[19] Y. Quan, X. Zhong, W. Feng, J. C. W. Chan, Q. Li, and M. Xing, "Smote-based weighted deep rotation forest for the imbalanced hyperspectral data classification," *Remote Sens (Basel)*, vol. 13, no. 3, pp. 1–25, Jan. 2021, doi: 10.3390/rs13030464.

[20] A. Özdemir, K. Polat, and A. Alhudhaif, "Classification of imbalanced hyperspectral images using SMOTE-based deep learning methods," *Expert Syst Appl*, vol. 178, Sep. 2021, doi: 10.1016/j.eswa.2021.114986.

[21] L. N. Eeti and K. M. Buddhiraju, "Classification Of Hyperspectral Remote Sensing Images By An Ensemble Of Support Vector Machines Under Imbalanced Data," in *IGARSS 2018-2018 IEEE International Geoscience and Remote Sensing Symposium*, IEEE, 2018, pp. 2659–2661.

[22] D. Datta, P. K. Mallick, J. Shafi, J. Choi, and M. F. Ijaz, "Computational Intelligence for Observation and Monitoring: A Case Study of Imbalanced Hyperspectral Image Data Classification," *Comput Intell Neurosci*, vol. 2022, 2022, doi: 10.1155/2022/8735201.

[23] M. Deák *et al.*, "Heterogeneous forest classification by creating mixed vegetation classes using EO-1 Hyperion," *Int J Remote Sens*, vol. 38, no. 18, pp. 5215–5231, 2017, doi: 10.1080/01431161.2017.1325529.

[24] S. A. Medjahed and M. Ouali, "A new hybrid SSA-TA: Salp Swarm Algorithm with threshold accepting for band selection in hyperspectral images," *Applied Soft Computing Journal*, vol. 95, 2020, doi: 10.1016/j.asoc.2020.106534.

[25] M. A. Toksöz and I. Ulusoy, "Hyperspectral Image Classification via Sparse Representation," *IEEE Transactions on Geoscience and Remote Sensing*, pp. 1–12, 2017.

[26] Q. Gao, S. Lim, and X. Jia, "Hyperspectral image classification using convolutional neural networks and multiple feature learning," *Remote Sens (Basel)*, vol. 10, no. 2, 2018, doi: 10.3390/rs10020299.

[27] M. P. Uddin, M. Al Mamun, and M. A. Hossain, "PCA-based Feature Reduction for Hyperspectral Remote Sensing Image Classification," *IETE Technical Review (Institution of Electronics and Telecommunication Engineers, India)*, vol. 38, no. 4. Taylor and Francis Ltd., pp. 377–396, 2021. doi: 10.1080/02564602.2020.1740615.

[28] B. Fang, Y. Bai, and Y. Li, "Combining spectral unmixing and 3D/2D dense networks with early-exiting strategy for hyperspectral image classification," *Remote Sens (Basel)*, vol. 12, no. 5, Mar. 2020, doi: 10.3390/rs12050779.

[29] M. P. Uddin, M. Al Mamun, and M. A. Hossain, "Effective feature extraction through segmentation-based folded-PCA for hyperspectral image classification," *Int J Remote Sens*, vol. 40, no. 18, pp. 7190–7220, Sep. 2019, doi: 10.1080/01431161.2019.1601284.

[30] N. Audebert, B. Le Saux, and S. Lefevre, "Deep learning for classification of hyperspectral data: A comparative review," *IEEE Geosci Remote Sens Mag*, vol. 7, no. 2, pp. 159–173, Jun. 2019, doi: 10.1109/MGRS.2019.2912563.

[31] H. Liu *et al.*, "Using t-distributed Stochastic Neighbor Embedding (t-SNE) for cluster analysis and spatial zone delineation of groundwater geochemistry data," *J Hydrol (Amst)*, vol. 597, Jun. 2021, doi: 10.1016/j.jhydrol.2021.126146.

[32] L. Gao, D. Gu, L. Zhuang, J. Ren, D. Yang, and B. Zhang, "Combining t-Distributed Stochastic Neighbor Embedding with Convolutional Neural Networks for Hyperspectral Image Classification," *IEEE Geoscience and Remote Sensing Letters*, vol. 17, no. 8, pp. 1368–1372, Aug. 2020, doi: 10.1109/LGRS.2019.2945122.